Hindawi
International Journal of Antennas and Propagation
Volume 2019, Article ID 7630815, 13 pages
https://doi.org/10.1155/2019/7630815

*Research Article*

# Beamwidth-Enhanced Low-Profile Dual-Band Circular Polarized Patch Antenna for CNSS Applications

**Hongmei Liu, Chenhui Xun, Shaojun Fang, and Zhongbao Wang**

*School of Information Science and Technology, Dalian Maritime University, Dalian 116026, China*

Correspondence should be addressed to Shaojun Fang; fangshj@dlmu.edu.cn

Received 11 June 2019; Revised 20 August 2019; Accepted 22 October 2019; Published 7 November 2019

Academic Editor: Ana Alejos



A low-profile dual-band circular polarized (CP) patch antenna with wide half-power beamwidths (HPBWs) is presented for CNSS applications. Simple stacked circular patches are used to achieve dual-band radiation. To enhance the HPBW for the two operation bands, a dual annular parasitic metal strip (D-APMS) combined with reduced ground plane (R-GP) is presented. A single-input feed network based on the coupled line transdirectional (CL-TRD) coupler is also proposed to provide two orthogonal modes at the two frequency bands simultaneously. Experimental results show that the 10 dB impedance bandwidth is 32.7%. The 3 dB axial ratio (AR) bandwidths for the lower and upper bands are 4.1% and 6.5%, respectively. At 1.207 GHz, the antenna has the HPBW of 123° and 103° in the *xoz* and *yoz* planes, separately. And the values are 127° and 113° at 1.561 GHz.

## 1. Introduction

Nowadays, satellite navigation systems are intensively used in various fields, such as navigation, public safety, and surveillance. The compass navigation satellite system (CNSS), officially named as the BeiDou Navigation Satellite System, has achieved more and more attention due to the navigation and positioning services compatible with other systems [1]. To receive signals with stable capacity, most satellite navigation systems use circularly polarized (CP) antennas. They have improved immunity to multipath distortion and polarization mismatch losses caused by Faraday rotation [2]. Among them, the CP microstrip antennas (CPMAs) have always been the research hotspot due to the advantages of low profile, light weight, and low cost. Besides, with the overall dimension of navigation system terminal getting smaller, compact CPMAs are highly demanded. Meanwhile, CPMAs with wide half-power beamwidths (HPBWs) are urgently required to improve the coverage area and stabilize the received signal.

Generally, metal back cavity [3–5] or the similar structure of back cavities [6] is applied to enhance the HPBW of CP antennas. However, they suffer from high profile, and their complex in geometry may lead to fabrication difficulties. Recently, a parasitic ring is stacked on the radiation patch to effectively widen the HPBW to 140° [7]. Parasitic strips [8] are also proposed to achieve wide HPBW. Nevertheless, these technologies [3–7] are presented for single-band applications.

In [9], a dual-band CPMA with wide HPBW is reported. By extending the substrate beyond the ground plane, the HPBWs of more than 100° and 114° are obtained at the two center frequencies. But the impedance and AR bandwidths are narrow. In [10], a dual-band CP antenna with enhanced beamwidth is proposed. By using stacked cone patches and a dual-ring cavity, the HPBWs are 135° and 112° at the two center frequencies. In [11], a compact dual-band CP antenna with wide HPBWs is proposed by using four compact inverted-F monopoles, and cross dipoles combined with the cavity-backed reflectors are also presented [12]. However, high profile, complex in geometry, and high cost are generated by the structure. Currently, dual-band CPMAs used for GPS [13] or BeiDou [14] satellite navigation applications are reported. In [13], a modified metallic cavity is presented for wide axial ratio beamwidth. In [14], stacked patches with dual circular polarizations are proposed. But both of them ignore the enhancement of the HPBWs. Therefore, it is essential to concentrate on improving the HPBW of a compact, low-profile dual-band CPMA.

In this paper, a compact dual-band CPMA resonates at CNSS B1 (1.561 GHz) and B2 (1.207 GHz) and is presented. To enhance the HPBW, a novel dual annular parasitic metal strip (D-APMS) combined with the reduced ground plane (R-GP) is presented. A compact single-input feed network based on the coupled line transdirectional (CL-TRD) coupler is also proposed to provide two orthogonal modes at the two frequency bands simultaneously. Detailed structures of the proposed antenna are presented in Section 2. In Section 3, the effects of the proposed D-APMS and R-GP are discussed and parametric studies are investigated. For demonstration, a prototype was fabricated and measured in Section 4. Comparisons are also presented between the design and some previous dual-band CP antennas, followed by a conclusion in Section 5.

## 2. Antenna Structure

Figure 1 shows the structure of the proposed antenna. It consists of three layers of substrates (top, middle, and bottom), two radiation patches (stacked patches), the D-APMS, the R-GP, and the CL-TRD-based feed network. Each of the three substrates has a relative permittivity of 3, a loss tangent of 0.003, and a thickness of 1.5 mm.

As shown in Figure 1(a), the stacked patches are designed as circular patches. The small circular patch with a radius of $R_1$, as the upper band main radiator, is printed on the upper surface of the top substrate. However, the big circular patch with a radius of $R_4$, as the lower band main radiator, is printed on the upper surface of the middle substrate. To improve the HPBW at the two operation bands, a novel D-APMS is printed on the upper surface of the top substrate (same layer as the small circular patch). The D-APMS is formed by a small APMS with an inner radius of $R_2$ and width of $d_5$ and a large APMS with an inner radius of $R_3$ and width of $d_6$. It is noted that the small and the large APMSs are divided into 4 sections by identical air gaps with the length of $d_3$ and $d_4$, respectively. The small APMS is used for improving the HPBW of the upper band, and the large APMS is contributed to the lower band. Moreover, to further enhance the HPBW, an R-GP with a radius of $R_5$ is etched on the top of the bottom substrate, as shown in Figure 1(b).

To provide two orthogonal modes on the stacked patches, a single-input feed network capable of simultaneously operating at the upper and lower bands is proposed, as shown in Figure 1(c). It consists of two CL-TRD couplers, a 90° phase shifter and a T-type power divider. The CL-TRD coupler, which is firstly introduced by Shie et al., can achieve tight coupling with weak coupled microstrip lines and allow decoupling the direct current path between the input and output ports [15]. Small size is also obtained compared with the branch-line coupler. In the design, a modified CL-TRD coupler [16] with improved power distribution and phase performance is applied to produce equal amplitude and consistent 90° phase shift. To suppress the mutual coupling between the upper and lower radiation patches, a 90° phase shifter is connected to the lower band CL-TRD coupler. Finally, a compact T-type power divider is used for connecting the two signal paths. As can be seen from Figure 1(c), the network provides four output ports (ports 2, 3, 4, and 5). The ports 2 and 3, with equal amplitude and 90° phase shift, are connected to the two short metal probes for feeding the lower band radiation patch, while the ports 4 and 5 are connected to the two long metal probes to feed the upper band radiation patch. Thus, two orthogonal modes on the two patches are excited, resulting in dual-band CP radiation waves. The input port (port 1) is connected to the coaxial cables. The modeling and simulation of the proposed antenna are performed with the 3D full-wave EM simulation software HFSS. Main dimension parameters of the antenna are listed in Table 1.

## 3. Design Procedure and Parametric Study

*3.1. Effects of APMS and R-GP.* To investigate the effects of APMS and R-GP on the HPBW of the CPMA, a single-band circular patch antenna working at 1.561 GHz is simulated. Here, four structures are compared, as shown in Figure 2. It starts from antenna 1, which is composed of a circular patch and a GP (the size of the GP is the same with that of the substrate). The antenna 2 is a circular patch antenna with an APMS etched on the same layer, while the size of the GP is also the same as that of the substrate. The antenna 3 is a circular patch antenna with an R-GP, and no APMS is used. The antenna 4 is a circular patch antenna with the combination of APMS and R-GP. It is noted that during the simulation, the dimensions of the substrate are fixed and the feed network is out of consideration. Moreover, the simulated results used for comparison are the optimal performances, including good impedance match (VSWR < 2), lowest AR, and widest HPBW.

Figure 3 shows the simulated HPBWs of the antenna in the *xoz* plane. It is observed that the HPBWs for antennas 1 and 2 are the narrowest. When an R-GP is etched, the HPBW is widened to 91°. A widest HPBW of 101° is obtained when using antenna 4, which means that the combination of APMS and R-GP can enhance the HPBW effectively. The current distributions along the radiation patch and the APMS, from $t = 0$ to $t = 3T/8$, are shown in Figure 4. It is observed that the antenna with the APMS still maintains the CP radiation and the electric field flows in an anticlockwise direction, yielding a right-hand circularly polarized (RHCP) wave in the upper half-space. The loaded APMS around the circular radiation patch serves as 4 directors which can lead part of the electromagnetic energy to the sides of the antenna. Therefore, the HPBW of the CP antenna is broadened.

*3.2. Discussions of D-APMS.* It is demonstrated from Section 3.1 that the APMS contributes to the HPBW enhancement of the CPMA. However, one APMS is valid for one frequency band. In order to enhance the HPBW at two operation bands, the D-APMS is applied, which is composed of two APMSs. In this section, the location and structure of the two APMSs are discussed to obtain the optimal HPBW.

Firstly, the locations of the two APMSs are investigated. In order to prove that the D-APMS is better than APMS for dual-band HPBW enhancement, the dual-band CPMA with

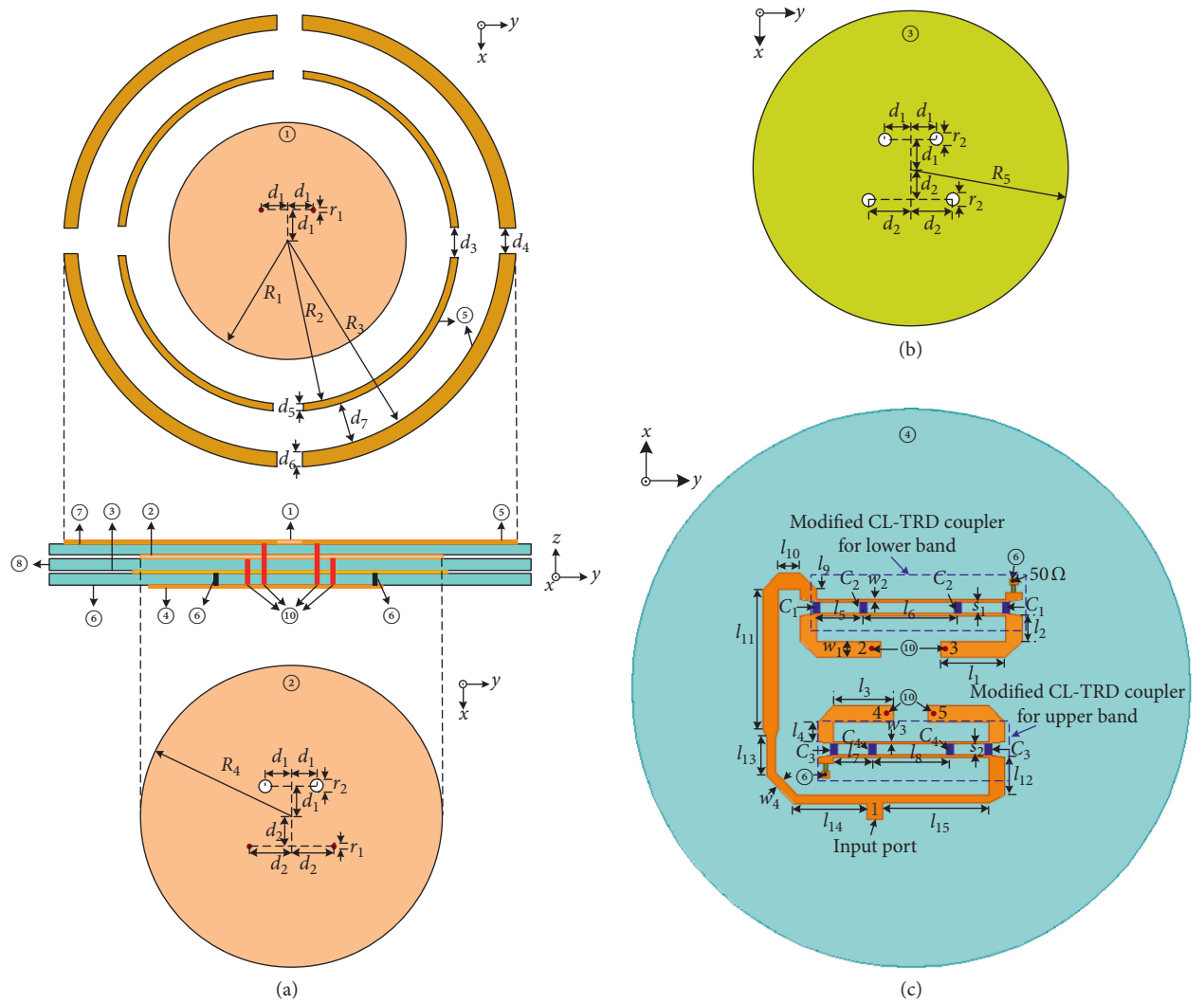


① Upper band radiation patch
② Lower band radiation patch
③ Reduced ground plane
④ Feed network
⑤ Dual annular parasitic metal strip
⑥ Via to ground
⑦ Top substrate
⑧ Middle substrate
⑨ Bottom substrate
⑩ Probe

Figure 1: Geometry of the proposed dual-band antenna. (a) Radiation patches with D-APMS. (b) R-GP. (c) Feed network.

Table 1: Dimension parameters of the proposed antenna (unit: mm and pF).

| | | | | mm | | | | | pF |
|---|---|---|---|---|---|---|---|---|---|
| $R_1$ | $R_2$ | $R_3$ | $R_4$ | $R_5$ | $r_1$ | $r_2$ | $w_1$ | $w_2$ | $C_1$ |
| 31.9 | 44 | 57.2 | 40.7 | 42.5 | 0.9 | 3 | 3.76 | 0.72 | 1.5 |
| $w_3$ | $d_1$ | $d_2$ | $d_3$ | $d_4$ | $d_5$ | $d_6$ | $d_7$ | $s_1$ | $C_2$ |
| 0.7 | 6 | 9 | 8 | 7 | 2.7 | 4 | 10.5 | 2.5 | 2.0 |
| $s_2$ | $l_1$ | $l_2$ | $l_3$ | $l_4$ | $l_5$ | $l_6$ | $l_7$ | $l_8$ | $C_3$ |
| 2.5 | 15 | 5.9 | 14 | 4.7 | 10.5 | 21 | 9 | 18 | 1.8 |
| $l_9$ | $l_{10}$ | $l_{11}$ | $l_{12}$ | $l_{13}$ | $l_{14}$ | $l_{15}$ | | | $C_4$ |
| 2.2 | 5 | 32.6 | 8.7 | 8 | 17.1 | 24.5 | | | 1.5 |

one APMS is also modeled and simulated. Figure 5 shows the different structures. In Figure 5(a), the APMS for the upper band (named as small APMS) is etched on the upper surface of the top substrate (same with the upper band radiator). In Figure 5(b), the APMS for the lower band (named as big APMS) is etched on the upper surface of the middle substrate (same with the lower band radiator). For location 1, as shown in Figure 5(c), the small APMS is located on the upper surface of the top substrate, while the big APMS is located on the upper surface of the middle substrate. For location 2, as shown in Figure 5(d), the two APMSs are both located on the upper surface of the top substrate. For location 3, as shown in Figure 5(e), the two APMSs are both located above the top substrate with a height of 1.5 mm, while the height is 3 mm for location 4, as shown in Figure 5(f).

Since the APMS is served as a parasitic radiation which is fed by air coupling from the main radiation patch, the size of the small and large APMSs, as well as the spacing between them, is related to the energy coupling strength caused by the

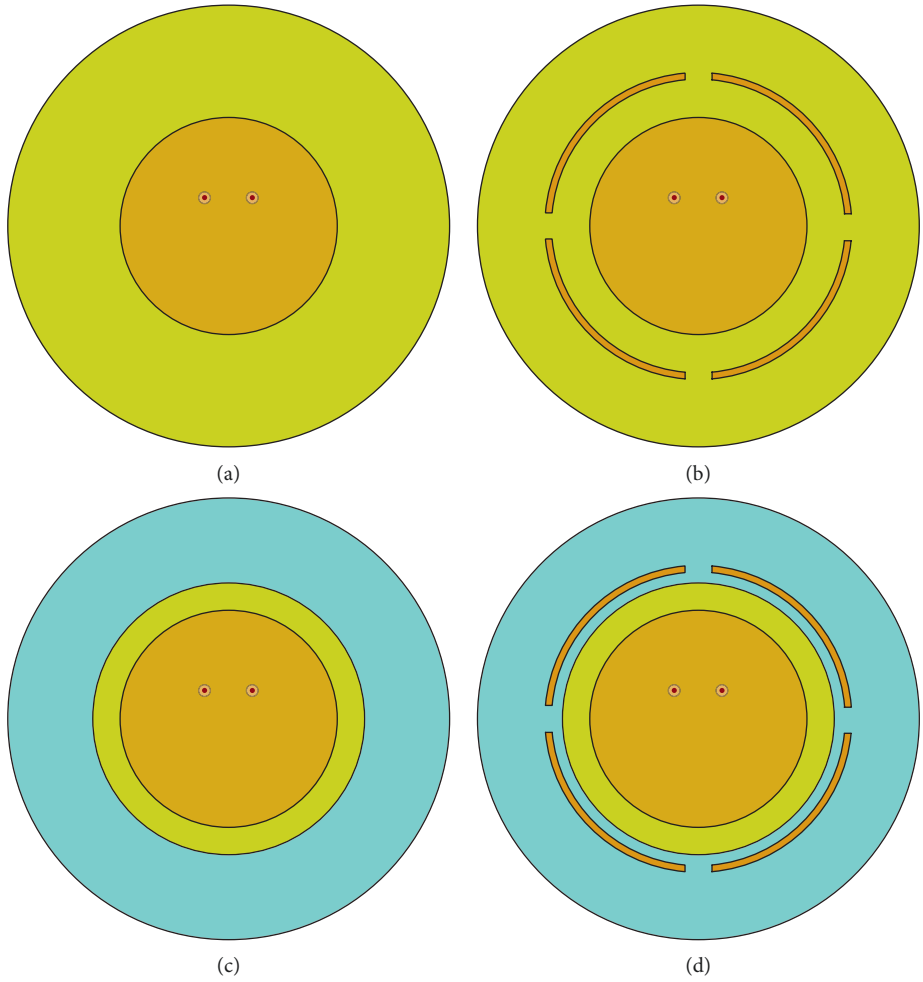


Figure 2: Single-band antenna with four structures. (a) Antenna 1. (b) Antenna 2. (c) Antenna 3. (d) Antenna 4.

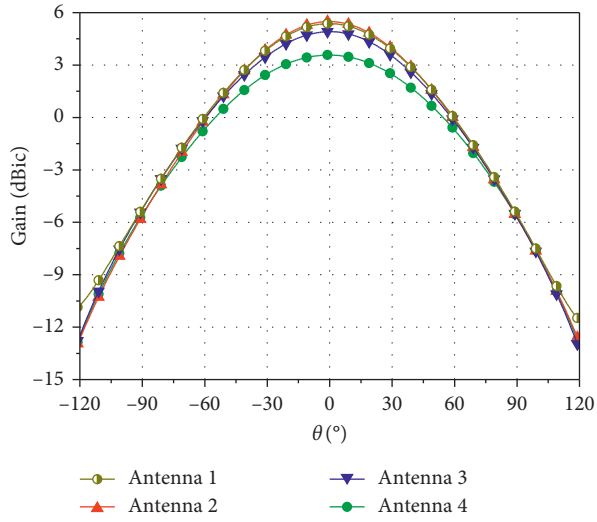


Figure 3: Radiation patterns for different antenna structures at 1.561 GHz.

air gaps. During the simulation, to obtain the widest HPBW for each state, the sizes of the APMSs are optimized. Figure 6 shows the simulated HPBW in the *xoz* plane at the two center frequencies. The radiation patterns for the dual-band CPMA without the APMS are also plotted for comparison (gray dashed dotted line). It is observed that the HPBWs are

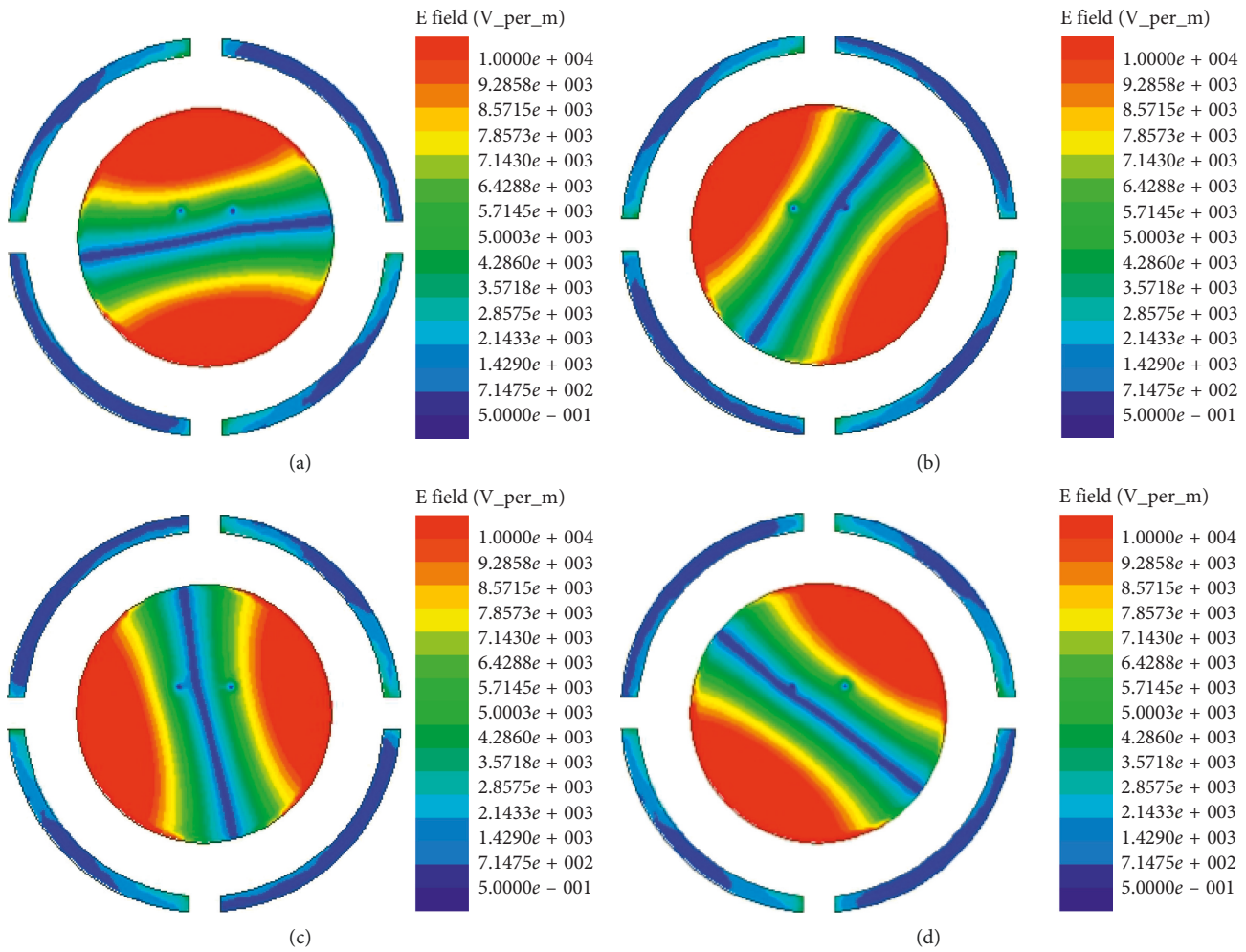


Figure 4: The current distributions over the antenna with the APMS at 1.561 GHz. (a) $t = 0$. (b) $t = T/8$. (c) $t = T/4$. (d) $t = 3T/8$.

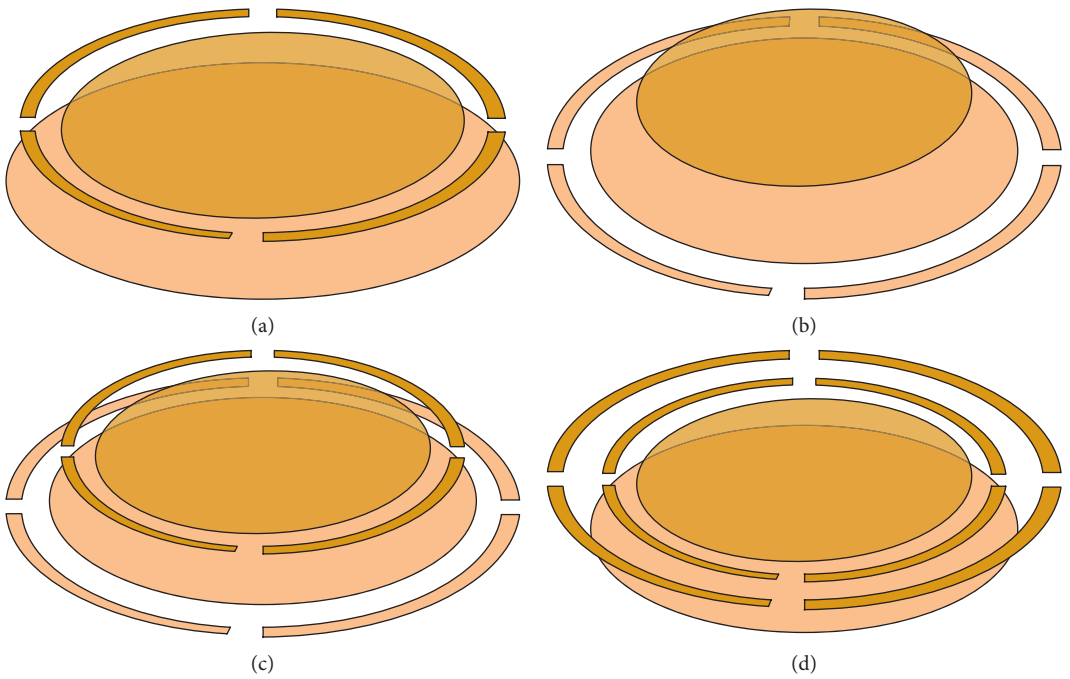


Figure 5: Continued.

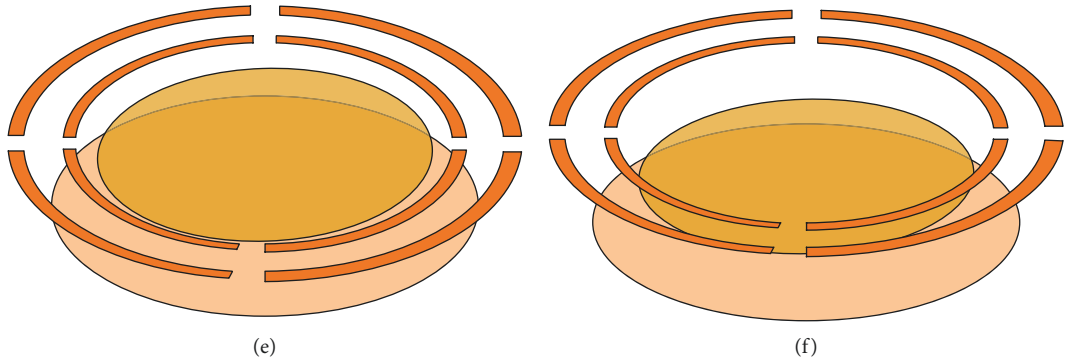


Figure 5: Different locations of the APMS. (a) With small APMS. (b) With large APMS (c) Location 1. (d) Location 2. (e) Location 3. (f) Location 4.

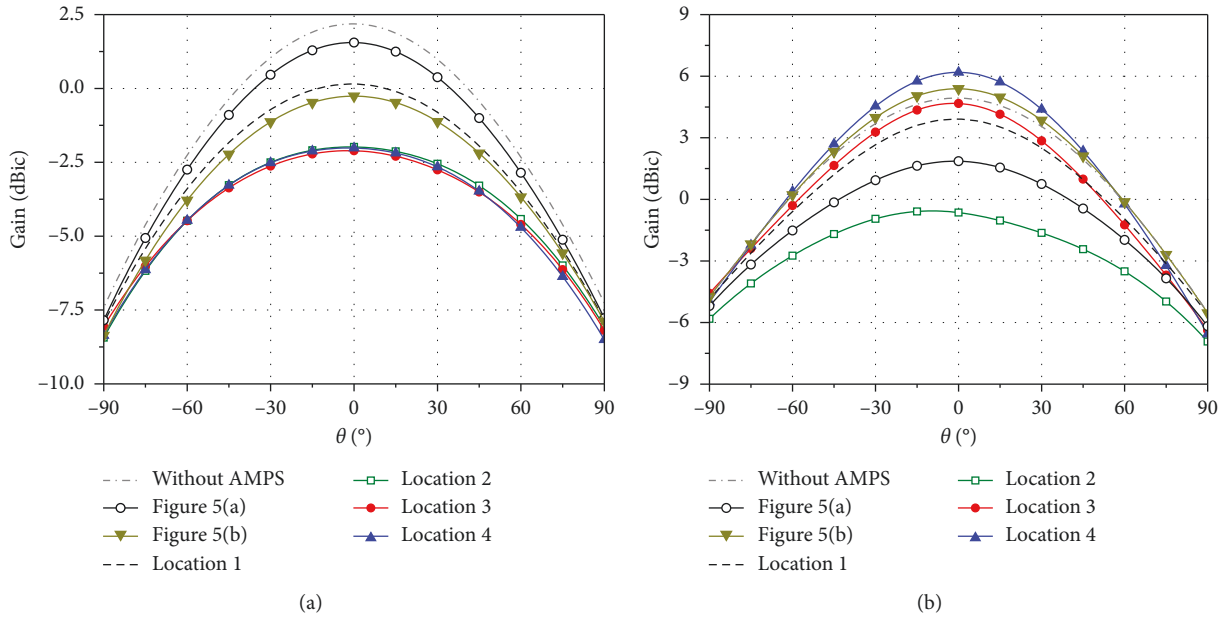


Figure 6: Radiation patterns for different locations of D-APMS. (a) 1.207 GHz. (b) 1.561 GHz.

97.2° and 92.1° for the lower and upper center frequencies, respectively. For the structure of Figure 5(a), the HPBWs at 1.207 GHz and 1.561 GHz are 98.8° and 108.4°, respectively, which indicate that the addition of small APMS contributes to the HPBW enhancement of the higher band and has less influence on the HPBW of the lower band. Considering the structure of Figure 5(b), the values of the HPBWs are 111.6° and 87.3°, which state that the addition of large APMS contributes to the HPBW enhancement of the lower band and can reduce the HPBW of the higher band. Thus, for dual-band HPBW enhancement, D-APMS should be applied.

For the different locations of the D-APMS, the simulated results can also be found in Figure 6. It is observed that, at 1.207 GHz, the HPBW for location 1 is the narrowest. The HPBW for locations 2, 3, and 4 are nearly the same. And a widest HPBW of 132° is obtained for location 3. At 1.561 GHz, the structure of location 2 shows wider HPBW (130°) than the others, while the beamwidths for locations 1, 3, and 4 are closer. In a comprehensive consideration, the optimal structure is the structure of location 2, where the two APMSs are located on the upper surface of the top substrate.

Secondly, the locations of the gaps on the D-APMSs are considered, as shown in Figure 7. It starts from Gap 1, where the gaps on the small and large APMSs are in the directions of 0°, 90°, 180°, and 270°. For Gap 2, as shown in Figure 6(b), the gaps on the large APMS are the same with Gap 1, while the gaps on the small APMS are rotated by 45°. For Gap 3, the gaps on the small APMS remain unchanged and the gaps on the large APMS are rotated by 45°. Figure 8 shows the simulated results. It is observed that the influence of the gaps on the small APMS is larger than that on the large APMS. At 1.207 GHz, the HPBWs for Gaps 1, 2, and 3 are 131°, 152°, and 108°, respectively. However, the values are 131°, 84°, and 85° at 1.561 GHz. Thus, the structure of Gap 1 is chosen.

Finally, the numbers of the gaps are discussed. Here, four states named as Strips 1, 2, 3, and 4 are investigated, as shown in Figure 9. For Strip 1, no gap is inserted to the APMS. For Strip 2, two gaps spacing 180° are added to the

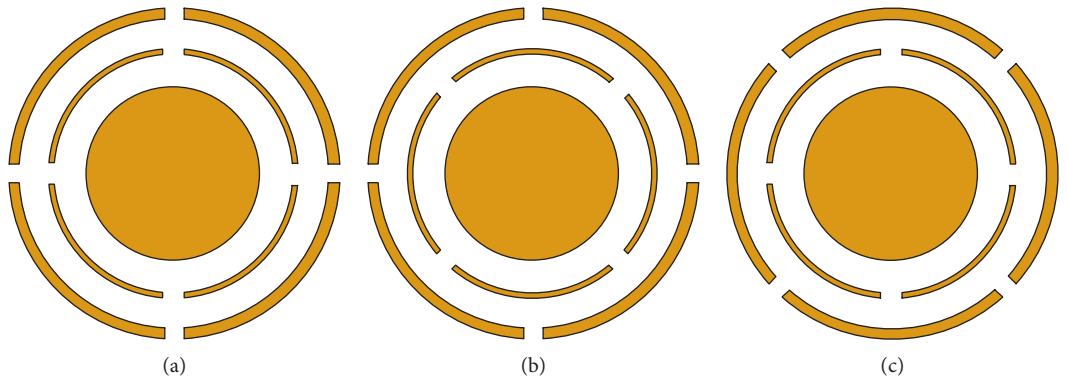


Figure 7: Different locations of the gaps on the two APMSs. (a) Gap 1. (b) Gap 2. (c) Gap 3.

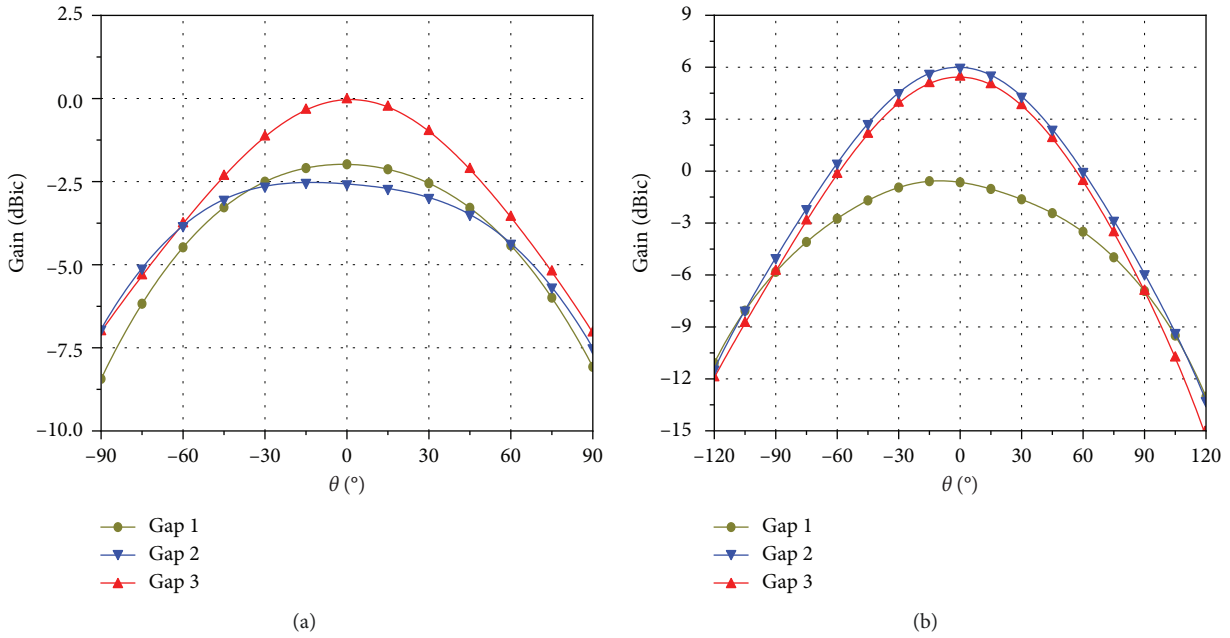


Figure 8: Radiation patterns for different locations of the gaps on the D-APMS. (a) 1.207 GHz. (b) 1.561 GHz.

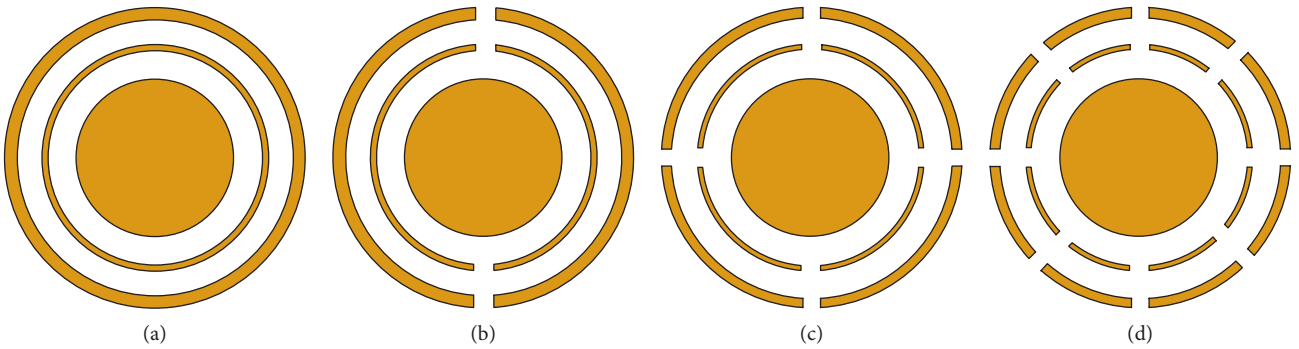


Figure 9: Different numbers of the strips. (a) Strip 1. (b) Strip 2. (c) Strip 3. (d) Strip 4.

APMS. For Strip 3, the interval between the gaps is 90°, while the value is 45° for Strip 4. Figure 10 shows the simulated HPBW at the two center frequencies. It is obvious that the antenna with Strip 3 shows the widest HPBW.

*3.3. Parametric Study.* In order to investigate the influence of the APMSs and the R-GP, a parametric study is carried out using HFSS. Figure 11(a) shows the effect of the width of the APMSs on the antenna HPBW. It is revealed that as the width of

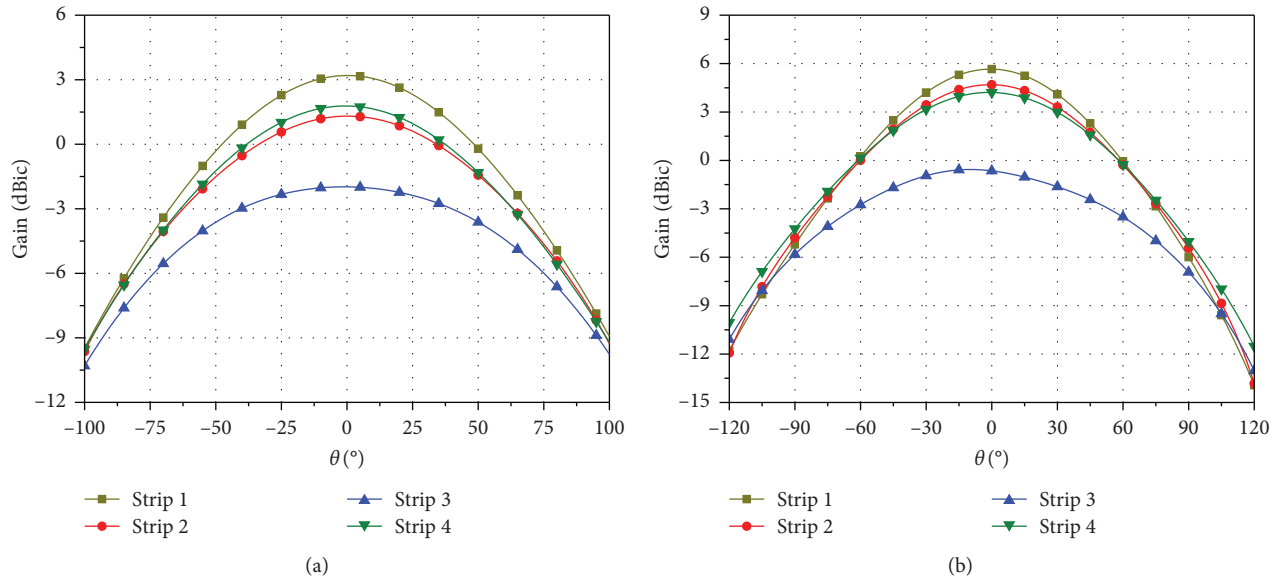


Figure 10: Radiation patterns for different numbers of gaps. (a) 1.207 GHz. (b) 1.561 GHz.

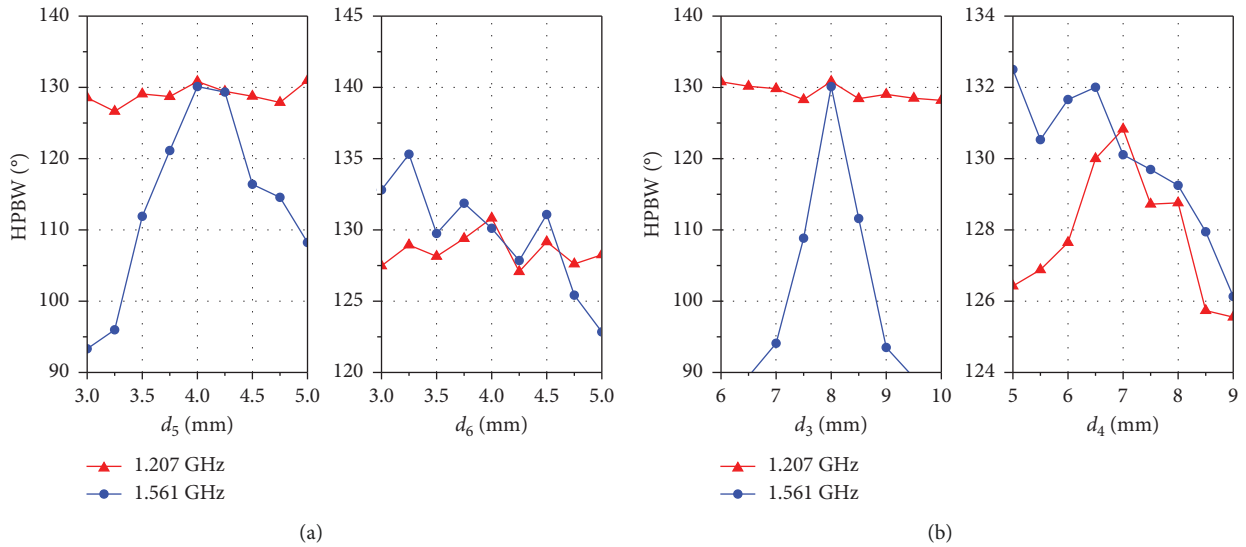


Figure 11: Effects of (a) the width and (b) the gap of the APMS on the HPBW.

the small APMS ($d_5$) increases from 3.0 to 4.0 mm, the HPBW at 1.561 GHz is increased, while when the width ($d_5$) increases from 4.0 to 5.0 mm, the HPBW is decreased. During the change in $d_5$, the HPBWs at 1.207 GHz are stable and are all larger than 125°. Thus, $d_5$ is determined to be 4.0 mm. When the width of the large APMS ($d_6$) is set to 4.0 mm, peak HPBW at 1.207 GHz is obtained, while the widest HPBW for 1.561 GHz is reached at $d_6 = 3.25$ mm. To balance the HPBW of the two center frequencies, the value of $d_6$ is chosen as 4.0 mm.

Figure 11(b) shows the effect of the gap of the APMSs on the antenna HPBW. It is observed that as the gap of small APMS ($d_3$) increases from 6 to 8 mm, the HPBW at the 1.561 GHz is increased. However, when $d_3$ increases from 8 to 10 mm, the HPBW is decreased. During the change in $d_3$, the HPBW at 1.207 GHz is stable. For the gap of the large APMS ($d_4$), peak HPBW is obtained at $d_4 = 7$ mm for 1.207 GHz.

Figure 12 shows the effect of the gap between the two APMSs and the dimension of the R-GP. It is seen that when the gap between the two APMSs ($d_7$) increases from 4.0 to 8.0, the HPBW at 1.561 is decreased, while the peak value of 131° is obtained at 1.207 GHz when $d_7 = 6.0$ mm. For the dimensions of R-GP, the optimal value is 43 mm.

## 4. Measurement Results

To validate the proposed design, a prototype is fabricated. Figure 13 shows the photograph of the prototype. The overall size is 130 mm × 130 mm × 4.5 mm. $|S_{11}|$ of the fabricated antenna is measured by using an Agilent N5230A vector network

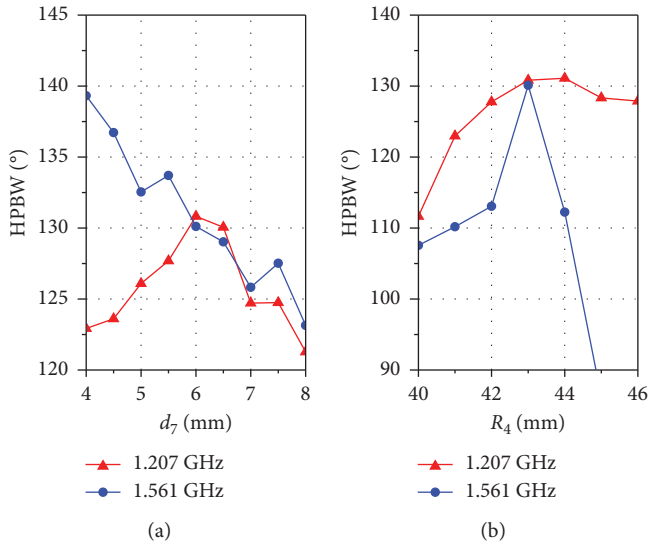


Figure 12: Effects of (a) the gap between the two APMSs and (b) the R-GP on the HPBW.

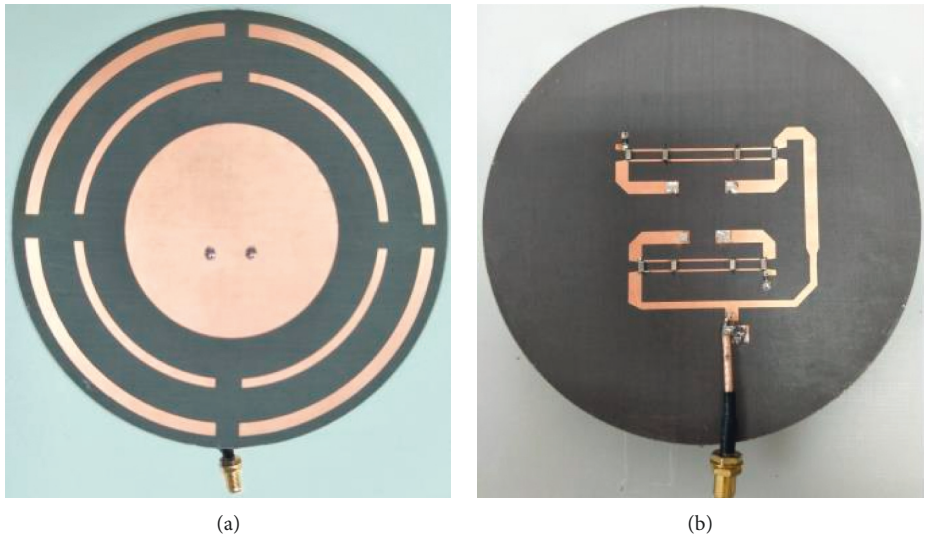


Figure 13: (a) Top and (b) bottom views of the fabricated prototype.

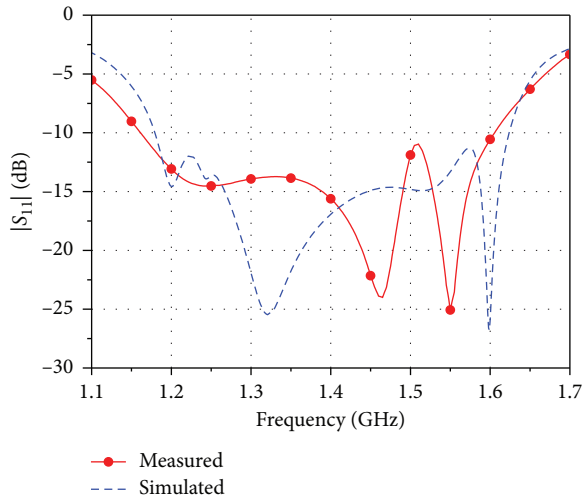


Figure 14: Measured and simulated $|S_{11}|$ of the fabricated antenna.

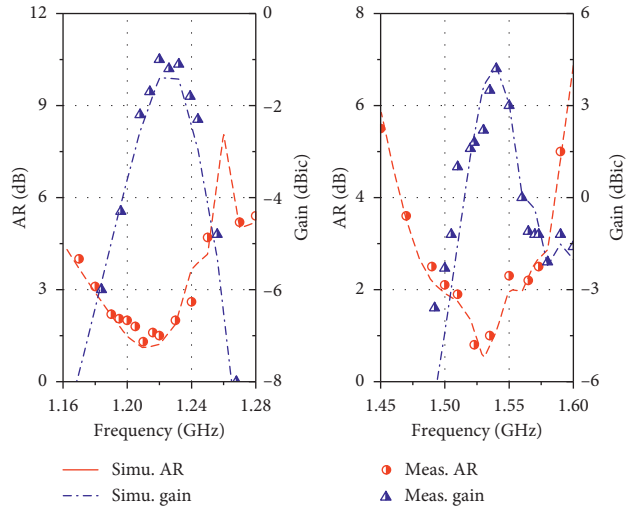


Figure 15: Measured and simulated gain and AR of the fabricated antenna.

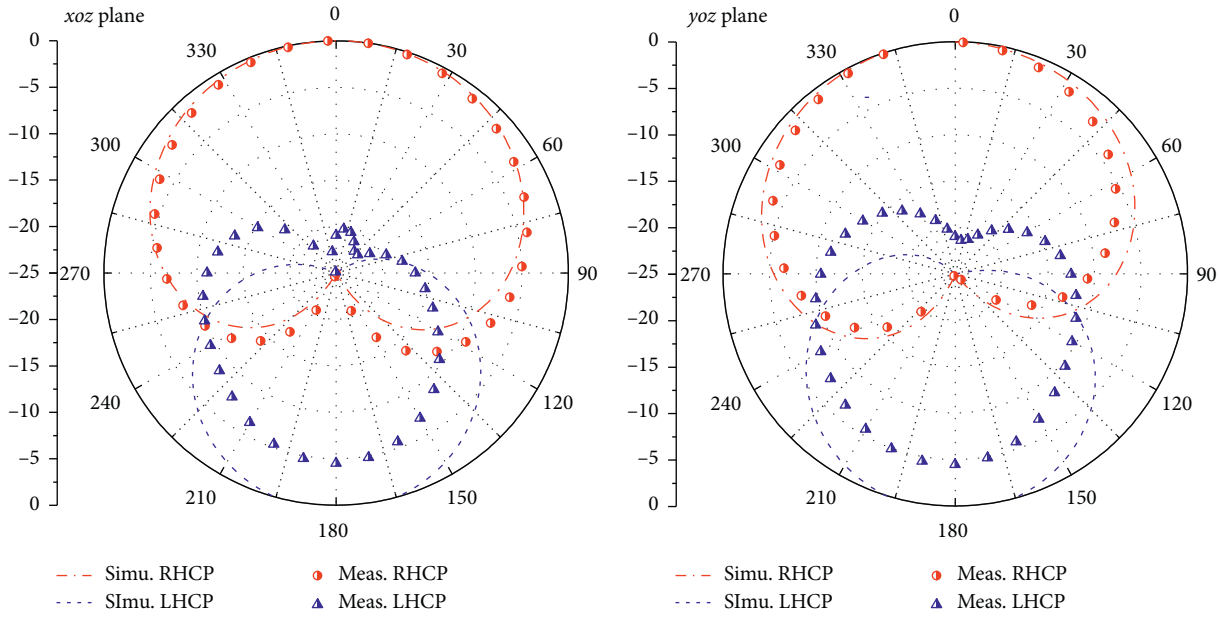


(a)

Figure 16: Continued.

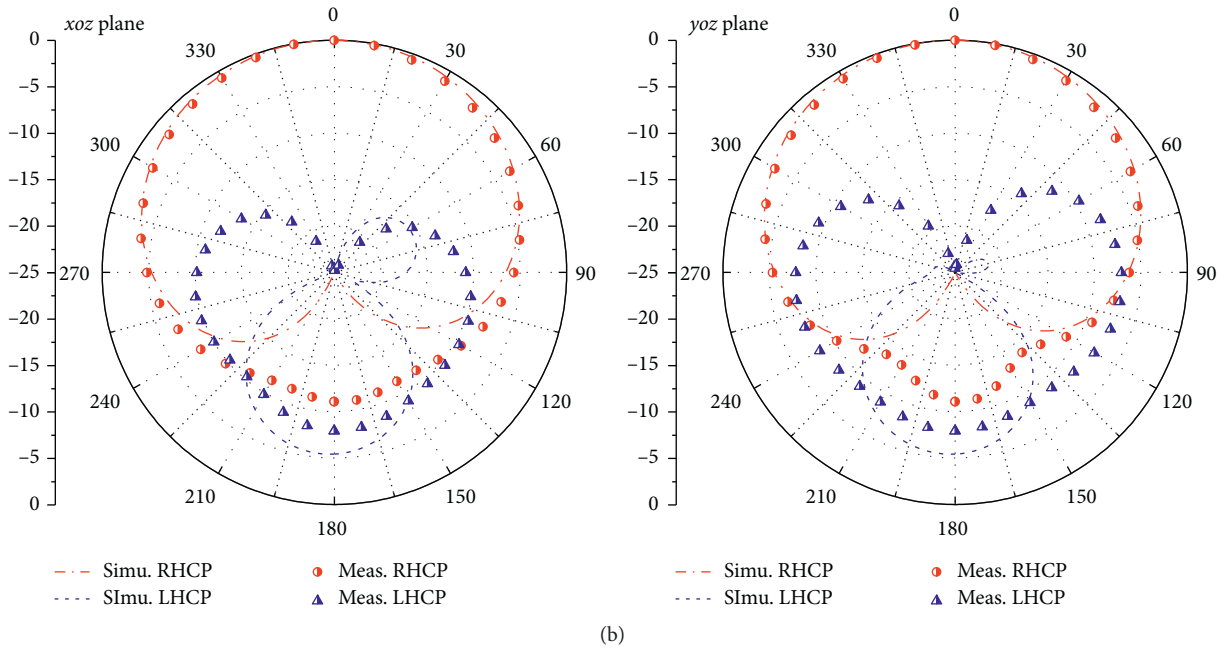


(b)

Figure 16: Measured and simulated normalized radiation patterns. (a) 1.207 GHz. (b) 1.561 GHz.

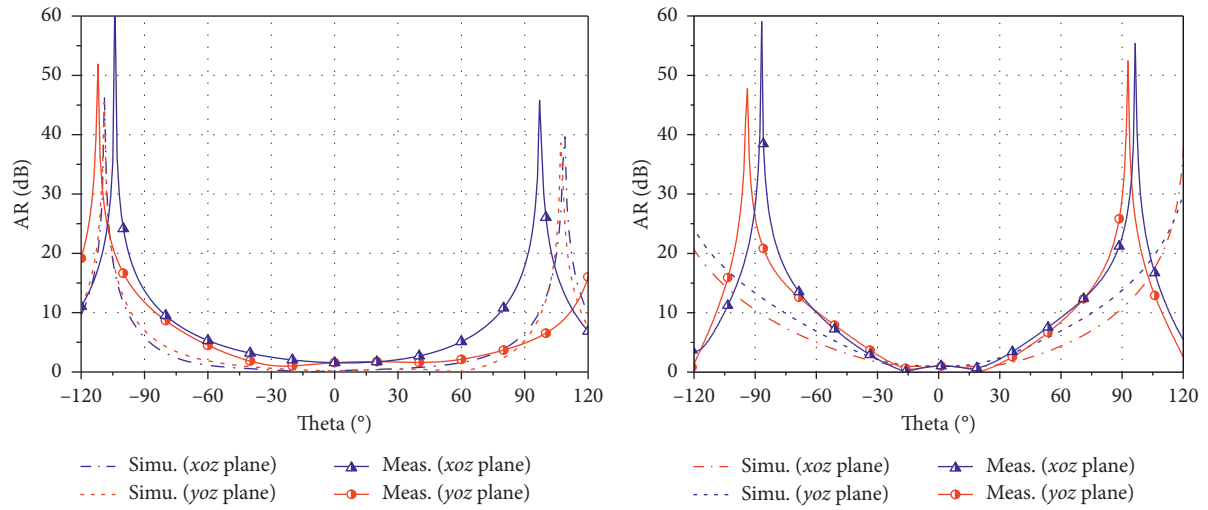


(a) (b)

Figure 17: Measured and simulated AR as a function of elevation angle in *xoz* and *yoz* planes. (a) 1.207 GHz. (b) 1.561 GHz.

analyzer. The far-field feature is measured in an anechoic chamber. Figure 14 shows the simulated and measured $|S_{11}|$ of the antenna. For $|S_{11}| < -10$ dB, the measured bandwidth is from 1.15 to 1.60 GHz. The differences between the simulated and measured $|S_{11}|$ may be caused by the fabrication errors. During the simulation, it is found that the gap error between the two patch layers may affect the performance of the antenna including $|S_{11}|$. Besides, the value error of the shunt commercial capacitors is another reason.

Figure 15 compares the measured and simulated gain and axial ratio (AR) at boresight. The measured minimum AR values of 1.3 and 0.6 are achieved at 1.21 and 1.53 GHz, respectively. For AR <3 dB, the measured bandwidths are 4.1% from 1.19 to 1.24 GHz for the lower band and 6.5% from 1.48 to 1.58 GHz for the upper band. In the frequency bands, the proposed antenna exhibits measured peak gains of −1 dBic at 1.207 GHz and 4.2 dBic at 1.54 GHz. The gain at 1.561 GHz is −0.6 dBic. It is observed that similar gains are obtained at the two resonated frequencies of CNSS. The reason for high gain at 1.54 GHz may be due to the HPBW reduction at the frequency point. From the analysis in Section 3, it is found that the gain is effectively increased with the decrease of the HPBW.

Figure 16 shows the simulated and measured radiation patterns of the antenna at 1.207 and 1.561 GHz. It is observed that symmetrical radiation patterns are exhibited at the two center frequencies. At 1.207 GHz, the measured HPBWs in the *xoz* and *yoz* planes are 123° and 103°,

Table 2: Comparisons between our design and previous dual-band CP antennas.

| Antenna | Overall size ($\lambda_0^3$) | Impedance bandwidth (%) | 3 dB AR bandwidth (%) | HPBW[a] |
|---|---|---|---|---|
| Ref. [9] | $0.483 \times 0.483 \times 0.015$ | 2.3<br>3.1 | 0.62<br>0.69 | 100°<br>114° |
| Ref. [10] | $0.524 \times 0.524 \times 0.224$ | ≥10<br>≥10 | ≥10<br>≥10 | 135°<br>112° |
| Ref. [11] | $0.211 \times 0.211 \times 0.057$ | 5.5<br>6.1 | 4.2<br>2.6 | 120°<br>116° |
| Ref. [12] | $0.573 \times 0.573 \times 0.296$ | 46.3 | 13.0<br>30.2 | 103°<br>111° |
| Ref. [13] | $0.368 \times 0.368 \times 0.105$ | 6.5<br>8.2 | Not given<br>Not given | 108°<br>107° |
| Ref. [14] | $0.38 \times 0.38 \times 0.024$ | 9.1<br>5.1 | 1.5<br>1.1 | <60°<br><60° |
| *This work* | **$0.523 \times 0.523 \times 0.018$** | **32.7** | **4.1**<br>**6.5** | **103°**<br>**113°** |

$\lambda_0$ is the wavelength in air at the lower center frequency. [a]The lower value in the *xoz* and *yoz* planes.

respectively. The values are 127° and 113° at 1.561 GHz. The measured and simulated ARs at 1.207 and 1.561 GHz in the *xoz* and *yoz* planes are plotted in Figure 17. The measured 3 dB AR beamwidths at 1.207 GHz are 82° and 123° in *xoz* and *yoz* planes, respectively, while the values are 72° and 94° at 1.561 GHz.

Table 2 compares our design with some previous dual-band CP antennas. It is observed that the proposed antenna exhibits similar HPBW with other antennas [9–12] at the upper center frequency. However, at the lower center frequency, the HPBW of the proposed antenna is smaller than those in [10, 11]. Although the antenna in [10] is better than the proposed structure, cavity has to be used, which increases design complexity and cost. In the item of impedance bandwidth and 3 dB AR bandwidth, the proposed antenna shows better performance than the antennas in [9, 11, 14]. However, compared with [10–13], the proposed antenna has smaller volume and lower profile. In summary, the proposed antenna features the characteristics of wider bandwidth and HPBWs with compact dimension and low profile.

## 5. Conclusion

In this study, a low-profile dual-band CPMA with wide HPBW is designed, fabricated, and measured. Wide HPBWs at the two bands are achieved with the proposed D-APMS and the R-GP. Moreover, with the employment of the CL-TRD-based feed network, wide impedance bandwidths are obtained. Among the published dual-band CP antennas with more than 100° HPBW for the navigation applications, the proposed CPMA has a wider bandwidth and a lower profile. Therefore, the proposed structure could be a good candidate for the dual-band CNSS applications to improve the system angular coverage.

## Data Availability

The data used to support the findings of this study are included within the article.

## Conflicts of Interest

The authors declare that there are no conflicts of interest regarding the publication of this paper.

## Acknowledgments

This work was supported in part by the National Natural Science Foundation of China (nos. 51809030, 61571075, and 61871417), China Post doctoral Science Foundation (no. 2017M611210), Doctor Startup Foundation of Liaoning Province (no. 20170520150), and Fundamental Research Funds for the Central Universities (nos. 3132019211 and 3132019219).

## References

[1] K.-K. Zheng and Q.-X. Chu, "A novel annular slotted center-fed BeiDou antenna with a stable phase center," *IEEE Antennas and Wireless Propagation Letters*, vol. 17, no. 3, pp. 364–367, 2018.

[2] K. Chen, J. Yuan, and X. Luo, "Compact dual-band dual circularly polarised annular-ring patch antenna for BeiDou navigation satellite system application," *IET Microwaves, Antennas & Propagation*, vol. 11, no. 8, pp. 1079–1085, 2017.

[3] X. H. Ye, M. He, P. Y. Zhou, and H. J. Sun, "A compact single-feed circularly polarized microstrip antenna with symmetric and wide-beamwidth radiation pattern," *International Journal of Antennas and Propagation*, vol. 2013, Article ID 106516, 7 pages, 2013.

[4] L. Chen, T.-L. Zhang, C. Wang, and X.-W. Shi, "Wideband circularly polarized microstrip antenna with wide beamwidth," *IEEE Antennas and Wireless Propagation Letters*, vol. 13, pp. 1577–1580, 2014.

[5] H. Jiang, Z. Xue, W. Li, and W. Ren, "Broad beamwidth stacked patch antenna with wide circularly polarised bandwidth," *Electronics Letters*, vol. 51, no. 1, pp. 10–12, 2015.

[6] S. He and J. Deng, "Compact and single-feed circularly polarised microstrip antenna with wide beamwidth and axial-ratio beamwidth," *Electronics Letters*, vol. 53, no. 15, pp. 1013–1015, 2017.

[7] Z. K. Pan, W. X. Lin, and Q. X. Chu, "Compact wide-beam circularly-polarized microstrip antenna with a parasitic ring for CNSS application," *IEEE Transactions on Antennas and Propagation*, vol. 62, no. 5, pp. 2847–2850, 2014.

[8] Y. Yuan, M. Wang, Y. F. Yin, and W. Wu, "Wide-beam circularly polarized microstrip antenna with high front-to back ratio for CNSS application," in *Proceedings of the 2017 Sixth Asia-Pacific Conference on Antennas and Propagation (APCAP)*, pp. 1–3, Xian, China, October 2017.

[9] X. L. Bao and M. J. Ammann, "Dual-frequency dual circularly-polarized patch antenna with wide beamwidth," *Electronics Letters*, vol. 44, no. 21, pp. 1233-1234, 2008.

[10] S.-L. Zuo, L. Yang, and Z.-Y. Zhang, "Dual-band CP antenna with a dual-ring cavity for enhanced beamwidth," *IEEE Antennas and Wireless Propagation Letters*, vol. 14, pp. 867–870, 2015.

[11] C. Li, F. S. Zhang, F. Zhang, and K. W. Yang, "A compact dual-band circularly polarized antenna with wide HPBWs for CNSS applications," *International Journal of Antennas and Propagation*, vol. 2018, Article ID 3563949, 10 pages, 2018.

[12] Y.-X. Sun, K. W. Leung, and J. Ren, "Dual-band circularly polarized antenna with wide axial ratio beamwidths for upper hemispherical coverage," *IEEE Access*, vol. 6, pp. 58132–58138, 2018.

[13] Z. P. Zhong, X. Zhang, J. J. Liang et al., "A compact dual-band circularly-polarized antenna with wide axial-ratio beamwidth for vehicle GPS satellite navigation applications," *IEEE Transactions on Vehicular Technology*, vol. 68, no. 9, pp. 8683–8692, 2019.

[14] H. Yang, Y. Fan, and X. Liu, "A compact dual-band stacked patch antenna with dual circular polarizations for BeiDou navigation satellite systems," *IEEE Antennas and Wireless Propagation Letters*, vol. 18, no. 7, pp. 1472–1476, 2019.

[15] C. I. Shie, J. C. Cheng, S. C. Chou, and Y. C. Chiang, "Transdirectional coupled-line couplers implemented by periodical shunt capacitors," *IEEE Transactions on Microwave Theory and Techniques*, vol. 57, no. 12, pp. 2981–2988, 2009.

[16] H. Liu, S. Fang, Z. Wang, and T. Shao, "Coupled line transdirectional coupler with improved power distribution and phase performance," in *Proceedings of the 2017 IEEE International Symposium on Radio-Frequency Integration Technology (RFIT)*, pp. 126–128, Seoul, South Korea, August 2017.